Highly Conducting Nanosized Monodispersed Antimony-Doped Tin Oxide Particles Synthesized via Nonaqueous Sol-Gel Method

Vesna Müller,[*] Jiri Rathousky,[**]Matthias Rasp,[*] Goran Štefanić,[***] Sebastian Günther,[*] Markus Niederberger,[****] and Dina Fattakhova-Rohlfing[*]

[*]Department of Chemistry and Biochemistry, University of Munich (LMU), Butenandtstrasse 5-13, 81377 Munich, Germany, Dina.Fattakhova@cup.uni-muenchen.de
[**]J. Heyrovsky Institute of Physical Chemistry, Academy of Sciences of the Czech Republic, Dolejskova 3, 182 23 Prague 8, Czech Republic, jiri.rathousky@jh-inst.cas.cz
[***]Division of Materials Chemistry, Ruđer Bošković Institute, P.O. Box 180, HR-10002 Zagreb, Croatia, stefanic@irb.hr
[****]Department of Materials, ETH Zürich, Wolfgang-Pauli-Strasse 10, 8093 Zürich, Switzerland, markus.niederberger@mat.ethz.ch

ABSTRACT

Conducting antimony-doped tin oxide (ATO) nanoparticles were prepared by a nonaqueous solution route, using benzyl alcohol as both the oxygen source and the solvent, and tin tetrachloride and Sb(III)/Sb(V) compounds as tin and antimony sources, respectively. This reaction produced non-agglomerated crystalline particles 3-4 nm in size, which can be easily redispersed in high concentrations in a variety of solvents to form stable transparent colloidal solutions without any stabilizing agents. The introduction of Sb dopant dramatically increased the particle conductivity, which reaches a maximum of $1 \cdot 10^{-4}$ S cm-1 for 4 % of Sb. Annealing in air at 500 °C further improves the conductivity to $2 \cdot 10^{2}$ S cm^{-1}.

Keywords: TCO, antimony-doped tin oxide, nanoparticles, conductivity, nonaqueous sol-gel synthesis

1 INTRODUCTION

Due to the unique combination of transparency in the visible range and high electric conductivity, transparent conducting oxides (TCOs) are widely used as electrodes in thin layer transparent devices such as solar cells, flat-panel displays, smart windows or electronics and chemical sensors. [1,2] Very recently, the focus of scientific attention has shifted from thin films to crystalline TCO nanoparticles. The use of nanocrystals opens the way to the deposition of conductive coatings by wet chemical methods at mild conditions, replacing expensive vacuum-based techniques and enabling coating temperature-sensitive plastic substrates. Moreover, such colloidal dispersions are of great interest for ink-jet printing technologies and are very attractive as primary building units for assembling nanostructured materials with defined porous architectures.[3]

Antimony-doped tin oxide (ATO) is a well-known transparent semiconductor with a large band gap of over 3.6 eV, providing transparency in the visible range and high n-type electric conductivity, which makes it a valuable alternative to much more rare and expensive indium tin oxide (ITO). ATO nanoparticles can be prepared by both chemical and physical methods, the former providing a much better control over the particle size and their stabilization in solution than the physical ones. In the present study we are reporting a nonaqueous-solution route to preparation of ATO nanoparticles with very small particle size, narrow size distribution and especially high electric conductivity.[4] Special emphasis was laid on good self-assembling properties of nanoparticles, as they are intended as suitable building blocks for the assembly of more complex nanoarchitectures. [5] The good electric properties of conducting oxides require an optimum doping level, a uniform distribution of the doping atom within the host lattice without phase separation and without any surface enrichment. Therefore, we have prepared ATO particles containing Sb in a wide range of concentrations, focusing on the effect of the nature and relative concentration of the metal oxide precursors and processing conditions on the structure, morphology and conductivity properties of the obtained nanoparticles. This synthetic approach provides ATO nanoparticles with exceptional properties such as small size, facile redispersibility in various solvents and high electric conductivity.

2 RESULTS AND DISCUSSION

In the synthesis of the ATO nanoparticles, anhydrous benzyl alcohol was used both as a solvent and as an oxygen source, and tin tetrachloride as the tin precursor. In order to test the influence of the nature of the antimony precursor on the doping efficiency and solubility of Sb in the tin oxide lattice, several commercially available antimony compounds with different antimony valence states and

various ligands were used, namely antimony (III) chloride, antimony (V) chloride, antimony (III) acetate and antimony (III) ethoxide. The rate of the particle formation and the particle yield greatly depend on the reaction temperature. While the reaction completion requires 20 h at 100 °C, only 2 h are sufficient if the temperature is increased to 150 °C. On the contrary, the nature of Sb precursor only marginally influences the mean particle size and its distribution, and the degree of agglomeration. For all the used precursors, the TEM images show practically non-agglomerated or only loosely agglomerated highly crystalline nanoparticles, as proven by lattice fringes in HRTEM and STEM (Fig. 1). The average size of the particles is about 3 nm and 4 nm if synthesized at 100 and 150 °C, respectively. Independently of the ligand nature, all the Sb(III) precursors provide similar non-agglomerated particles exhibiting narrow particle size distribution. The use of precursors more reactive towards solvolysis, such as of $SbCl_5$, leads to some acceleration of the particle formation reaction, slight increase in the particle size and an increased amount of agglomerated nanoparticles.

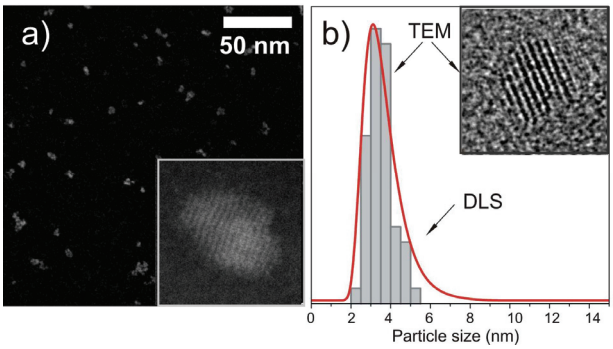

Figure 1. Morphology, size and dispersibility of 10 % ATO nanoparticles prepared using $Sb(ac)_3$ at 150 °C: (a) STEM-HAADF image. The inset 6 x 6 nm in size show high resolution STEM-HAADF images of a single nanoparticle. (b) Size distribution of nanoparticles determined from HRTEM images (gray bars) and from DLS measurement (red line) of a colloidal dispersion in EtOH of the same nanoparticles. The inset 6 x 6 nm in size shows high resolution TEM image of a single nanoparticle.

With regard to the properties of obtained ATO particles, the solubility limit of Sb dopant in the SnO_2 lattice and the influence of the dopant concentration on the structure, crystallinity, size and the conductivity of the formed ATO particles are of primary importance. Therefore, we prepared the particles containing from 0 to 50 mol % of Sb using $Sb(ac)_3$ as antimony source. Synthesis without any addition of antimony results in the formation of white particles. The color of the obtained particles changes to brownish-green when an Sb source is added to the reaction mixture. Besides the change in color, an increase in Sb content leads to the acceleration of the particle formation and an increase in the particle yield, which is especially pronounced at lower reaction temperatures.

The particles can be easily redispersed at high concentration of about 3-8 wt% in different solvents without the addition of any surface-stabilizing agent, such as water, ethanol or THF, to form stable transparent colloidal solutions. The particles in the solution are practically non-agglomerated and show a narrow size distribution, as determined by DLS (Fig. 1b). The dispersibility of the antimony-doped nanoparticles is much better than that of the pristine SnO_2 ones. Moreover, it is worse in more polar solvents such as water, but is greatly improved by the addition of a few drops of concentrated hydrochloric acid. Such a striking difference could originate from the different surface charge of the particles with the varying Sb content, and points out the significant role of electrostatic effects in the colloid's stabilization.

The XRD patterns of ATO nanoparticles with an Sb content up to 30 mol% show the presence of only one crystalline phase structurally closely related to cassiterite, which indicates that the SnO_2 lattice can accommodate up to 30 mol% of Sb atoms without significant changes in the structure. The first indication of a second crystal phase ($Sb_4O_5Cl_2$) appears only at a very high Sb concentration of 40 mol%. Solid solubility limit of antimony ions in the cassiterite lattice is approximately 38 mol%, as estimated from the dependence of the diffraction line intensities of the $Sb_4O_5Cl_2$ phase on the initial content of Sb, and by extrapolation to the zero intensity. With increasing antimony content peaks corresponding to the cassiterite structure become broader as a result of the decrease in particle size from 4.3 nm for the undoped sample to 4.1 nm and 4.0 nm for samples with 10 mol% and 20 mol% of antimony, respectively, in good agreement with the results obtained by TEM. The incorporation of Sb ions causes an asymmetric distortion of the cassiterite lattice due to the difference in the ionic radii of the Sn^{4+} ion (0.69 Å in coordination 6) and antimony ions (0.76 Å and 0.61 Å in coordination 6 for Sb^{3+} ion and Sb^{5+} ion, respectively). Estimated values of unit-cell parameters of cassiterite (0% ATO) and cassiterite-type solid solutions (10 % ATO and 20 % ATO) obtained from the Le Bail and Rietveld refinements of XRD patterns show that the increase in the antimony content cause a linear decrease of parameter *a* and a linear increase of parameter *c*.

The phase composition of the ATO particles was further studied by Raman spectroscopy, which is able to deliver structural information on amorphous and poorly crystalline samples and is very sensitive to the presence of even minor amounts of crystalline phases. The typical bulk vibration modes predicted by group theory for the SnO_2 rutile structure, namely A_{1g} (630 cm^{-1}), B_{2g} (775 cm^{-1}) and E_g (477 cm^{-1}), are observed for the undoped SnO_2 sample although with low intensity, probably due to the small particle size. Moreover, the spectra of the samples containing up to 40 mol% of antimony show the bands corresponding to the rutile type of SnO_2. Position of these

bands shifts with the increasing antimony content, indicating the influence of the replacement of Sn with Sb within the lattice. A_{1g} and B_{2g} modes corresponding to the vibrations perpendicular to the c axis decrease in intensity and shift to lower wave numbers with increasing antimony content, while the E_g mode corresponding to the vibration in direction of c axis follows the opposite trend. This continuous change in the vibration modes of the doped oxides is in good agreement with the XRD data, which also prove the slight asymmetric distortion of the crystalline SnO_2 lattice due to the incorporation of Sb ions. No bands corresponding to antimony oxides were found for the samples containing up to 40% Sb. Strong bands of the antimony (III) oxide were observed only for the sample containing 50 mol% Sb. All the spectra of ATO particles feature an intense band at 333 cm^{-1} and bands between 500 and 570 cm^{-1}. They were often observed for nanosized tin oxides, being frequently assigned to the surface vibration modes of tin oxide. The intensity of these bands changes with increasing antimony content, which can be related to vibration modes of incorporated antimony atoms inside the cassiterite lattice.

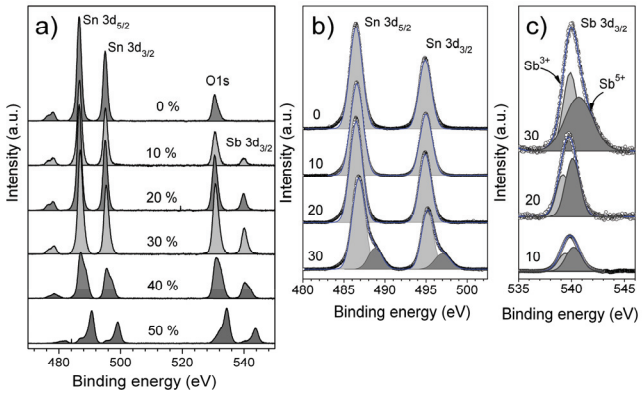

Figure 2. X-ray photoelectron spectra (XPS) of the as prepared ATO nanoparticles with varying Sb content synthesized at 150 °C using $Sb(ac)_3$ as an antimony source: overview spectra for the energy region between 460 and 560 eV (a) and the sections corresponding to the Sn_{3d} doublet (b) and Sb $3d_{3/2}$ antimony peaks (c). The solid lines correspond to the experimental spectra, and the open circuits and the grey shaded areas are the fitted curves and the Gaussian peak fits of the individual elements, respectively.

Conductivity of the ATO nanoparticles depends to a large extent on the antimony content and its oxidation state in the tin oxide lattice. While Sb^{5+} ions act as electron donors forming a shallow donor level close to the conduction band of SnO_2, Sb^{3+} behaves as an electron acceptor. If both oxidation states coexist, which is often observed for ATO materials, the resistivity is given by the ratio of Sb^{5+} and Sb^{3+} sites, which was analyzed by X-ray photoelectron spectroscopy (XPS). The overview spectra (Fig. 2a) obtained for the ATO samples demonstrate the strong peaks corresponding to Sn (Fig. 2b) and to oxygen and antimony (Fig. 2c). The total Sb content determined by the surface-sensitive XPS method is practically the same as that obtained by the bulk-sensitive energy-dispersion X-ray spectroscopy EDX method, indicating that particle composition is homogeneous throughout the complete particle without any enrichment of the surface of the nanoparticles with Sb atoms. In addition, as we have found all the particles independently of the Sb content contain ca. 60% of Sb^{5+} and 40% of Sb^{3+}, the effective donor Sb^{5+} concentration exceeds that of the acceptor by 20 % (effective n-type doping).

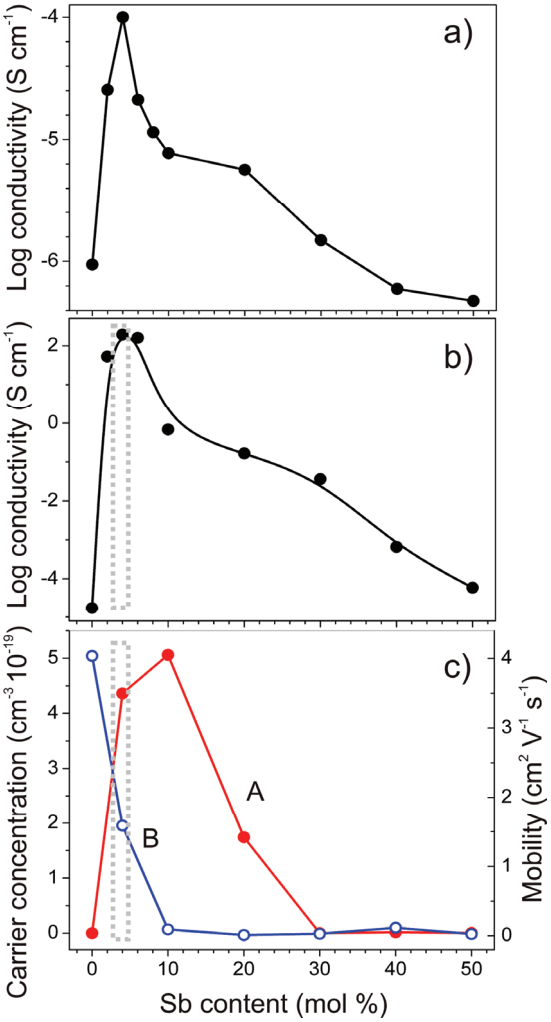

Figure 3. Conductivity (log scale) of the pellets pressed from ATO nanoparticles synthesized at 150 °C containing different Sb concentration using $Sb(ac)_3$ as antimony precursor: as prepared (a) and after calcination in air at 500 °C (b). For the latter, corresponding charge carrier concentration (A) and charge carrier mobility (B) are shown in (c).

Electrical conductivity of the ATO nanoparticles measured in pressed pellets strongly depends on the Sb content. The conductivity of the pure SnO_2 sample is very low, being only $9 \cdot 10^{-7}$ S cm^{-1}. The conductivity dramatically increases due to the introduction of small amounts of Sb, reaching a maximum for the 4 % ATO nanoparticles. Further increase in Sb content leads to a deterioration of the electrical conductivity, samples containing more than 20 mol % exhibiting conductivity comparable to or even worse than the undoped SnO_2 (Fig. 3a). To the best of our knowledge, the obtained conductivity of $1 \cdot 10^{-4}$ S cm^{-1} is the highest ever reported for non-annealed ATO particles only a few nm in size.

The pellets conductivity further increases by four orders of magnitude after their calcination at 500 °C in air (Fig. 3b). The thermal treatment mainly leads to particle sintering and removal of organic impurities, providing good electrical contact between them, and to some extent to an increase in the particle size. The calcined pellets exhibit a similar effect of the Sb content on the conductivity, but at a much higher conductivity level.

The dependence of the charge carrier concentration on the Sb content in our ATO particles exhibits a pronounced maximum for the Sb concentration of 4-10 % (Fig. 3c), which is attributed to the formation of a shallow donor level close to the conduction band of SnO_2. For even higher Sb contents the carrier concentration decreases, as the increased disorder raises the effective activation energy of the donor. Even more strongly than the charge carrier concentration, the carrier mobility is affected by the variation of the dopant concentration, rapidly decreasing with the introduction of rather small amounts of antimony. As the XRD, Raman and TEM experiments have shown, the particle size decreases and the lattice disorder increases with the increasing Sb content. This contributes to the increased effects of grain boundary scattering, and ionized impurity and optical lattice scattering mechanisms, which are the reasons of the deteriorated charge carrier mobility in doped samples. Consequently, the best performance of the sample with 4 mol% of antimony is the result of the optimum combination of the high charge carrier concentration and high mobility inside the lattice.

3 CONCLUSIONS

Conducting ATO nanoparticles were prepared by a nonaqueous solution route, using benzyl alcohol, tin tetrachloride and a suitable Sb(III) compound. The non-agglomerated particles 3-4 nm in size are easy to redisperse in a variety of solvents to form stable transparent colloidal solutions without any stabilizing agents. The increase in antimony content causes a continuous decrease in particles size and a slight asymmetric distortion of the cassiterite SnO_2 lattice. The particle composition is homogeneous throughout the whole volume, without any enrichment of the surface with Sb atoms. Introduction of Sb dopant dramatically increases the particle conductivity, which reaches a maximum for 4 % of Sb being more than two orders of magnitude higher than that of the pristine SnO_2 nanoparticles. The conductivity further improves to ca. $2 \cdot 10^2$ S cm^{-1} due to particle sintering during annealing in air at 500 °C.

The combination of exceptional virtues makes the developed ATO nanoparticles an ideal material for electrostatic applications or as conducting additive for both organic and inorganic composites. As such, colloidal solutions of conducting nanoparticles are of special interest for direct printing of patterned electrodes. Above all, the reported ATO particles are attractive building blocks for assembling transparent conducting 3-D architectures, which offer favorable extra properties in comparison to those of traditional conducting layers. The high crystallinity of the nanoparticles serving as building blocks enables to obtain the fully crystalline inorganic frameworks with sufficient electric conductivity and high thermal stability already at temperatures as low as 300 °C without any need for the elaborate post-synthetic treatment. [5] Owing to the open and accessible character of porosity, the high surface area and the uniform pore size, the obtained mesoporous frameworks are the ideal host materials for the accommodation of functional redox moieties. The high potential of the obtained mesoporous layers as nanostructured transparent electrodes with the high surface area was demonstrated on an example of ferrocene molecules which were covalently immobilized in the conducting matrix, showing the greatly enhanced electrochemical response proportional to the electrode surface area. [5]

ACKNOWLEDGEMENT

The authors are grateful to the German Research Foundation (DFG, grant No. FA 839/1-1) and the Grant Agency of the Czech Republic (grant No. 104/08/0435-1) for the financial support.

REFERENCES

[1] D. Fattakhova Rohlfing, T. Brezesinski, J. Rathouský, A. Feldhoff, T. Oekermann, M. Wark, B. Smarsly, Adv. Mater. 18, 2980, 2006.

[2]. D. Fattakhova-Rohlfing, T., B. Smarsly, J. Rathouský, Superlattices and Microstructures 44, 686, 2008.

[3] J.M. Szeifert, D. Fattakhova-Rohlfing, D. Georgiadou, V. Kalousek, J. Rathousky, D. Kuang, S. Wenger, S.M. Zakeeruddin, M. Grätzel, T. Bein, Chem. Mater. 21, 1260, 2009.

[4] V. Müller, M. Rasp, G. Štefanić, J. Ba, S. Günther, J. Rathousky, M. Niederberger, D. Fattakhova-Rohlfing, Chem. Mater. 21, 5229, 2009.

[5] V. Müller, M. Rasp, J. Rathousky, M. Niederberger, D. Fattakhova-Rohlfing:, Small, 2010, 6, 633.